

Strong dissipation of steep swells observed across oceans

Fabrice Ardhuin

Service Hydrographique et Océanographique de la Marine, Brest, France

Bertrand Chapron

Laboratoire d'Océanographie Spatiale, Ifremer, Centre de Brest, Plouzané, France

Fabrice Collard

Collecte Localisation Satellites, division Radar, Plouzané, France

Global observations of ocean swell propagation is presented and analyzed, using on four years of satellite Synthetic Aperture Radar data. Tracking swells along their propagation paths yields an estimation of the dissipation of their energy. Swells can be very persistent with energy e-folding scales exceeding 30,000 km. For increasing swell steepness, this scale shrinks down to 2700 km, revealing a significant loss of swell energy. This pattern is consistent with a laminar to turbulent transition of the boundary layer, induced by the opposite wave-induced motions of air and water, with a threshold Reynolds number of the order of 100,000. This finding opens the way for more accurate wave forecasting models, and provides a constraint on swell-induced air-sea fluxes of momentum and energy.

1. Introduction

Swells are surface waves that outrun their generating wind, and radiate across ocean basins. Wind-waves that radiate away from their generation area dissipate and grow in length over a relatively short distance [Snodgrass *et al.*, 1966], say 2000 km. Further away, these waves closely follow principles of geometrical optics, with a constant wave period along geodesics, when following a wave packet at the group speed [e.g. Snodgrass *et al.*, 1966]. These geodesics are great circles along the Earth surface, with minor deviations due to ocean currents. As it takes a longer fetch or a faster wind to develop higher and longer waves, swells recorded by in situ measurements have been used to estimate the positions and intensity of generating storms across the oceans [Munk and Snodgrass, 1957]. The longest swells are thus fingerprints of the most powerful ocean storms.

Because swells are observed to propagate over long distances, their energy should be conserved or weakly dissipated [Snodgrass *et al.*, 1966]. As a matter of fact, very little quantitative information is available on this topic. Due to this poor knowledge, swells are relatively poorly predicted [Rogers, 2002]. Numerical wave models that neither account specifically for swell dissipation, nor assimilate wave measurements, invariably overestimate significant wave heights (H_s) in the tropics [Tolman, 2002; Bidlot *et al.*, 2005; Rascl *et al.*, 2008]. Typical biases in the most recent of these models reach 45 cm or 25% of the mean observed wave height in the East Pacific [Bidlot *et al.*, 2005; Rascl *et al.*, 2008]. Further, modelled peak periods along the

North American west coast exceed those measured by open ocean buoys, on average by 0.8 s [Rascl *et al.*, 2008], indicating that these models have too much long period energy where swells are more important. Previously proposed swell dissipation parameterizations, based on empirically adjusted wind-wave numerical simulations [Chalikov, 1993; Tolman, 2002], on the contrary lead to underestimations, up to 0.8 s, of peak periods in the Pacific. Swell evolution over large scales is thus not understood.

Swells are also observed to modify air-sea interactions [Grachev and Fairall, 2001; Sullivan *et al.*, 2008]. It is estimated that 3 TW of swell energy are eventually dissipated on shorelines [Rascl *et al.*, 2008], but it is not known how much may be lost between the intense storms where they are generated and the coasts. Swell energy is thus a potential source of ocean mixing [Babanin, 2006]. A quantitative knowledge of the swell energy budget is thus needed both for marine weather forecasting and Earth system modelling.

The only experiment that followed swell evolution at oceanic scales was carried out in 1963. Using in situ measurements, a very uncertain but moderate dissipation of wave energy was found, only for waves with period $T \leq 13$ s [Snodgrass *et al.*, 1966]. The difficulty of this type of analysis are twofold. First, very few storms produce swells that line up with any measurement array, and second, large errors are introduced by having to account for island sheltering. Qualitative investigations by Holt *et al.* [1998] and Heimbach and Hasselmann [2000] demonstrated that a space-borne synthetic aperture radar (SAR) could be used to track swells across the ocean, building on the coherent persistence of swells along their propagation tracks. Here we make a quantitative analysis of four years of global SAR measurements, from the European Space Agency's (ESA) ENVISAT platform. The dataset quality is discussed in section 2, and the swell analysis method is presented in section 3. The resulting estimates of swell dissipation are interpreted in section 4, and conclusions follow in section 5.

2. Quality of SAR parameters obtained from ENVISAT wave mode

Over the ocean, the nominal SAR acquisition mode of ESA satellites, the wave mode, was specifically designed to provide a sparse but global coverage of swells. Wave Mode imagettes are 5 by 10 km radar scenes acquired every 100 km looking to the right of the flight direction, 23° from nadir. Taking advantage of improvements in SAR processing, with the use of inter-look cross spectra [Engen and Johnsen, 1995] that removes the 180° directional ambiguity and considerably reduces the noise, ESA has been producing a level 2 (L2) product from the wave mode data, that contains the directional spectrum of waves. The swell significant height

H_{ss} peak period T_p and peak direction θ_p can all be estimated from the spectrum.

Contrary to other methods for estimating the wave spectrum [e.g. Hasselmann et al., 1996; Schulz-Stellenfleth et al., 2005], no wave model information is used in the L2 processing [Chapron et al., 2001], and the only outside information is the ocean surface wind direction, taken from analyses from the European Center for Medium Range Weather Forecasting (ECMWF). All SAR data used here are L2 products, provided by ESA and obtained with the processor version operational at ESA since November 2007. For data before this date, we used archive data reprocessed from level 0, using that same processor version, because previous versions insufficiently filtered non-wave signatures in the radar images, often causing low wavenumber artefacts [Johnsen and Collard, 2004].

For swell, SAR-derived peak periods and directions are very accurate [Holt et al., 1998; Johnsen and Collard, 2004]. Yet, the quality of the retrieved H_{ss} is paramount because we wish to determine the loss of swell energy $E_s = 4\sqrt{H_{ss}}$. Previous validations were presented for the total wave height H_s [Collard et al., 2005] or a truncated wave height H_{s12} defined using a fixed frequency cut-off at 1/12 Hz. For that parameter Johnsen and Collard [2004] found an r.m.s. error of 0.5 m, which includes a bias of 0.2 m, when comparing SAR against buoy data. In our study we use H_{ss} values obtained from both SAR and buoy spectra using a method similar to that of Gerling [1992]. A preliminary validation of H_{ss} was performed by Collard et al. [2006], using L2 processing applied to 4 by 4 km tiles from narrow swath images exactly located at buoy positions. That study found a 0.37 m r.m.s.

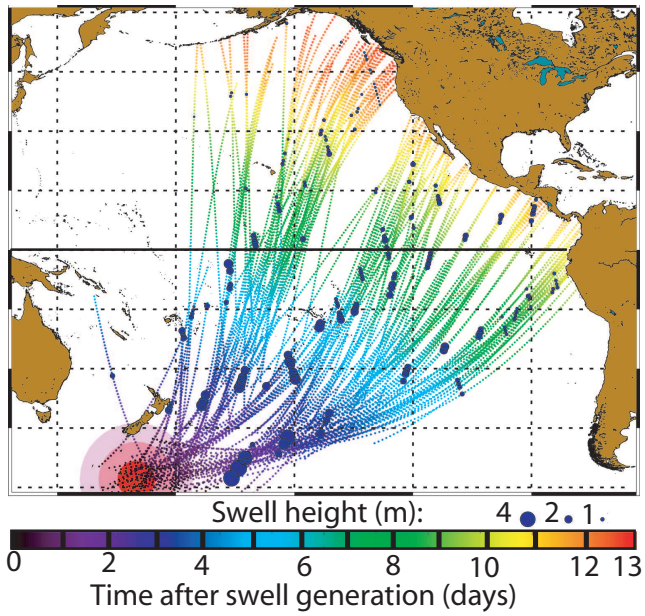


Figure 1. Finding the storm: Focussing of swells observed from space. All swells with a 17 ± 0.5 s period that were identified in 13 days of ENVISAT synthetic aperture radar data over the Pacific, are re-focussed from their location of observation (filled dots) following their direction of arrival at the theoretical group speed for 17 s waves. This focussing reveals a single swell generation event, well defined in space and time (pink to red disks). The back-tracking trajectories are color-dated from black (July 9 2004 18:00 UTC) to red (July 22 2004 18:00 UTC).

error, which includes a 0.17 m bias. This smaller error was obtained in spite of a 4 times smaller image size, suggesting that a significant part of the "errors" in other SAR validation studies are due to the distance between SAR and buoy data.

The validation of H_{ss} is repeated here, using buoys located within 100 km and 1 hour of the SAR observation, and 100 km or more from the coast or shallow water. After selecting buoys with good quality spectra, 2148 swell partitions were obtained with wind speeds between 1 and 10 m s^{-1} . Overall the bias is 0.24 m and the standard deviation of the errors is 0.5 m. The bias is found to be primarily a function of the swell height and wind speed, increasing with height and decreasing with wind speed. Variations in standard deviation are instead dominated by the swell height and peak period, with the most accurate estimations for large periods. When the distance between the buoy and SAR data is reduced to 50 km, only 100 data points are

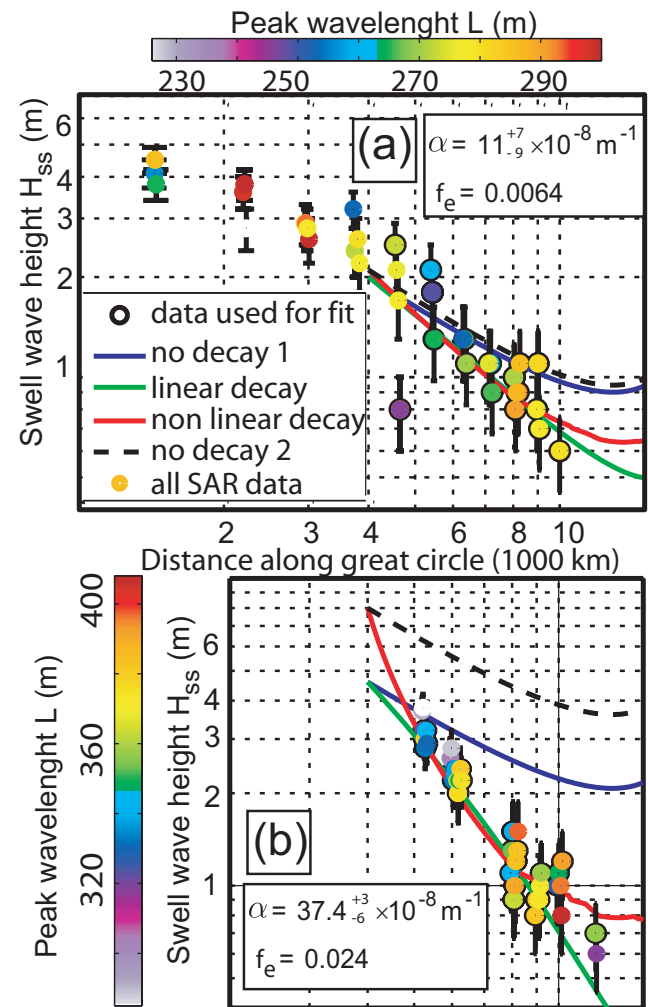


Figure 2. (a) Observed swell wave height as a function of distance, and theoretical decays with fitted coefficients using no dissipation, linear or non-linear dissipation, for the 13 s waves generated by Typhoon Ting-Ting. Circled dots are the observations used in the fitting procedure. Error bars show one standard deviation of the expected error on each SAR measurement. (b), Same as (a) for steeper swells observed in February 2007.

available, but the overall standard deviation decreases to 0.4 m.

Based on these results, a conservative error model for the SAR-derived H_{ss} is a gamma distribution with a bias given by

$$H_{ss} - \mu = 0.1H_{ss} - 0.15 \max\{0, U_{10} - 7\} \quad (1)$$

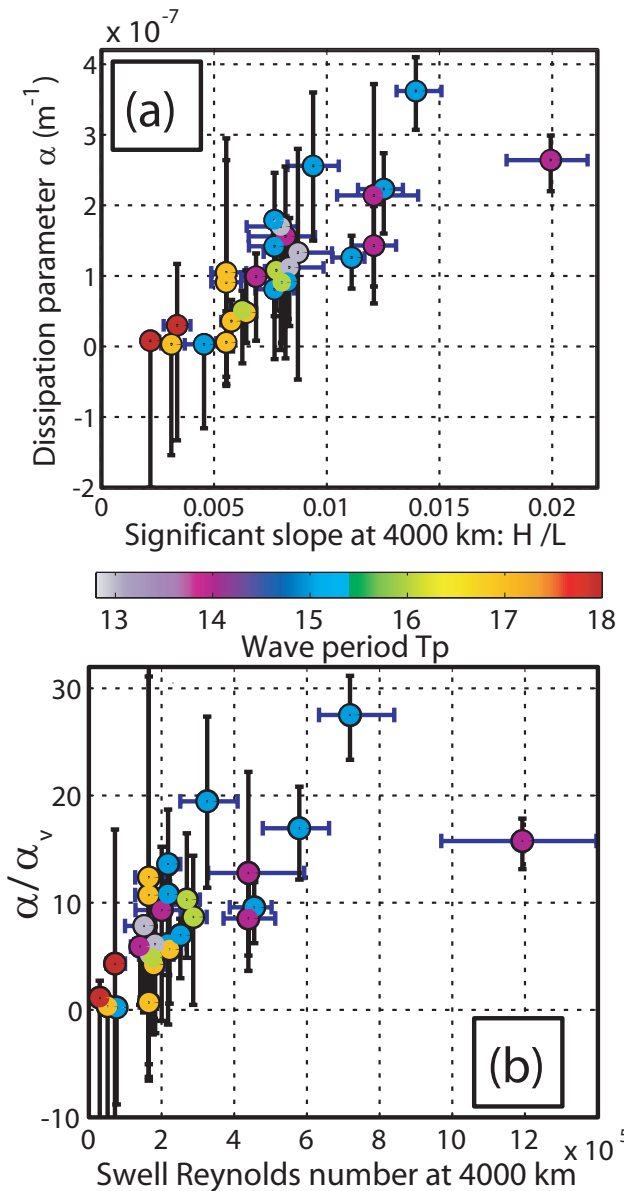


Figure 3. Swell dissipation for 29 events. (a) Estimated linear attenuation coefficient as a function of the initial significant slope, ratio of the significant wave height and the peak wavelength, $s = 4H_s/L$, taken 4000 km from the storm centre, for a variety of peak swell periods (colors). (b) Attenuation coefficient normalized by the viscous attenuation α_v (eq. 2), as a function of the swell Reynolds number Re_s determined from r.m.s. velocity and displacement amplitudes at 4000 km from the storm.

where μ is the expected value of H_{ss} in meters and the wind speed U_{10} is in m s^{-1} , and a standard deviation given by

$$\sigma = \max \{0.15, \min \{0.25H_{ss}, 0.4\}\} \quad (2)$$

where σ and H_{ss} are in meters. A more simple model, with larger errors based on the H_{s12} analysis by *Johnsen et al.* [2006], does not significantly alter the following analysis.

3. Swell tracking and dissipation estimates

Our analysis uses a two step method. Firstly, using SAR-measured wave periods and directions at different times and locations, we follow great circle trajectories backwards at the theoretical group velocity. The location and date of swell sources is defined as the spatial and temporal center of the convergence area and time of the trajectories. This preliminary step provides a global view of swell fields in both space and time. In figure 1, a swell covers one Earth quadrant away from the storm, with a large detection gap that extends from the Southern Pacific to California. This blank area is the long shadow cast by French Polynesia where wave energy is dissipated in the surf [e.g. *Tolman*, 2003].

Secondly, we track the swells forward in space and time, starting from the source at an angle θ_0 , and following ideal geodesic paths in search of SAR observations. Great circle tracks are traced from the source in all directions, except for angular sectors with islands. Along each track, all SAR data are selected if they are acquired within 3 hours and 100 km from the theoretical position. In a first filtering procedure, we retain only SAR-derived swell partitions with peak wavelength and direction within 50 m and 20° of their theoretical values when assuming a point source. Tracks with neighboring values of the outgoing direction θ_0 were merged in relatively narrow direction bands (5 to 10° aperture) in order to increase the number of observations along a track, yielding 29 track ensembles.

If no energy is lost by the wave field, the spectral density $F(f, \theta, \varphi, \theta_0)$ is constant along the propagation path, where $f = 1/T$ is the wave frequency, θ is the local wave propagation direction, and φ is the separation angle, from the source, on the spherical Earth. A stationary storm that generates a broad wave spectrum yields a swell energy per unit ocean surface $E_s(\varphi, \theta_0) = \int \int F(f, \theta, \varphi, \theta_0) df d\theta$, in which the integration is over the swell partition only. E_s decreases asymptotically as $1/[\varphi \sin(\varphi)]$ away from the source [Munk et al., 1963, see also auxiliary information, discussion 2]. The $\sin(\varphi)$ factor arises from the initial spatial expansion of the energy front, with a narrowing of the directional spectrum. The φ factor is due to the dispersive spreading of the energy packet, because the group speed C_g is inversely proportional to the wave period, associated to a narrowing of the frequency spectrum. In each track ensemble, all swells have close initial directions θ_0 , and the wave field is only a function of φ . We define the spatial evolution rate

$$\alpha = -\frac{dF(f, \theta, \varphi)/d\varphi}{RF(f, \theta, \varphi)}, \quad (3)$$

where R is the Earth radius. Positive values of α correspond to losses of wave energy (Figure 2.b).

The swell dissipation scale for each ensemble was then estimated by finding the constant dissipation factor α , defined in eq. (3), that minimized the mean quadratic difference between theoretical and observed swell height decays. In each ensemble, some SAR data were filtered out (see 'Methods' in auxiliary information): This removed all the data within 4000 km of the originating storm to make sure that the remaining data are in the far field of the storm, where, in the

absence of dissipation, the energy decays asymptotically as $1/[\varphi \sin(\varphi)]$. The uncertainty on α was estimated using 400 synthetic data sets in which the swell wave heights were perturbed using the error model given by eq. (1)-(2). Similarly, a non-linear dissipation function with a constant value of the dissipation factor f_e (eq. 5) was also fitted to the data, using a numerical wave model (see auxiliary information).

We find that α ranges from -0.6 to $3.7 \times 10^{-7} \text{ m}^{-1}$ (Figure 3.a), comparable to $2.0 \times 10^{-7} \text{ m}^{-1}$ previously reported for large amplitude swells with a 13 s period [Snodgrass *et al.*, 1966]. Clarifying earlier observations by *Darbyshire* [1958] and *Snodgrass et al.* [1966], our analysis unambiguously proves that swell dissipation increases with the wave steepness.

4. Interpretation of swell dissipation

At present there is no consensus on the plausible causes of the loss of swell energy [WISE Group, 2007]. Interaction with oceanic turbulence was once thought to be the prime source of swell dissipation, but it is now expected to be relatively small [Ardhuin and Jenkins, 2006]. Observed modifications and reversals of the wind stress over swells [Grachev and Fairall, 2001] suggest that some swell momentum is lost to the atmosphere. The wave-induced modulations of stresses yield a flux of energy from the waves to the wind, due to the correlations of pressure and velocity normal to the sea surface, and the correlations of shear stress and tangential velocity. Both can yield an upward flux of momentum, readily observed over steep laboratory waves, in the form of a wave-driven wind [Harris, 1966]. In recent models of airflows over waves, these modulations have been linearized [e.g. Kudryavtsev and Makin, 2004], so that the swell dissipation rate is linear in terms of the wave energy, and cannot increase with the swell steepness.

Because our observation show no clear trend with wind magnitude and direction, we take a novel approach, and interpret our data by neglecting the effect of the wind, considering only the shear stress modulations induced by swell orbital velocities. Little data is available for air flows over swells, but boundary layers over fixed surfaces are much better known, and should have similar properties if their significant orbital amplitudes of velocity and displacement are doubled (see auxiliary information discussion 4). The flow should thus depend on the surface roughness and a significant Reynolds numbers, $\text{Re}(\varphi) = 4u_{\text{orb}}(\varphi)a_{\text{orb}}(\varphi)/\nu$.

For $\text{Re} < 10^5$, the flow is expected to be laminar [Jensen *et al.*, 1989], and the viscous effects should be dominated by the strongly sheared thin oscillatory boundary layer, in the air. The viscous dissipation coefficient is given by Dore [1978]

$$\alpha_\nu = 2 \frac{\rho_a 2\pi}{\rho_w C_g L} \sqrt{4\pi\nu/T}, \quad (4)$$

where L is the swell wavelength, $L = gT^2/(2\pi)$ in deep water with g the acceleration of gravity. At ambient temperature and pressure, the air viscosity is $\nu = 1.4 \times 10^{-5} \text{ m}^2\text{s}^{-1}$, and α_ν is only a function of T . As T increases from 13 to 19 s, α_ν decreases from 2.2×10^{-8} to $5.8 \times 10^{-9} \text{ m}^{-1}$.

For larger Reynolds number the flow is expected to be turbulent. Following common practice, the energy rate of decay in time is

$$\beta = C_g \alpha = \frac{\rho_a 4\pi^2}{\rho_w g T^2} f_e u_{\text{orb}} \quad (5)$$

where f_e is a non-dimensional swell dissipation factor, of the order of 0.002 to 0.008 for a smooth surface [Jensen *et al.*, 1989], when f_e is assumed equal to the friction factor f_w .

Re is difficult to estimate from the SAR data only, because ENVISAT's ASAR does not resolve the short windsea

waves. However, in deep water we can define the smaller 'swell Reynolds number' Re_s from $u_{\text{orb},s} = 2\sqrt{E_s} 2\pi/T$ and $a_{\text{orb},s} = 2\sqrt{E_s}$. For reference, a 6.3 m s^{-1} wind generates short waves with $\text{Re} = 2 \times 10^5$, making the boundary layer turbulent for any swell amplitude.

Our estimates of α exceed α_ν by a factor that ranges from $O(1)$ to 28 (Figure 3.b). Our results thus presents quantitative similarities with oscillatory boundary layer over fixed surfaces with no or little roughness. Namely, dissipation rates α of the order of the viscous value α_ν are found for $\text{Re}_s < 5 \times 10^4$ when the flow may be laminar, and we only find large values of α/α_ν when $\text{Re}_s > 5 \times 10^4$ over a significant portion of the swell track (figure 3.b). Using a numerical wave model, this value of Re_s translates to $\text{Re} \simeq 10^5$. Using modelled values of u_{orb} and fitting a constant f_e for each set of observations, yields $0.001 \leq f_e \leq 0.024$, with a median of 0.009, close to what is expected over a smooth surface.

Intuitively, winds should modify the boundary layer over swell, but may only dominate for winds larger than 7 m s^{-1} (auxiliary information discussion 3). Kudryavtsev and Makin [2002] considered the wind stress modulations due to short wave roughness modulated by swells, and found. Yet, their linear model cannot explain the nonlinear dissipation observed here, because they only considered lowest order effects. Further investigations should probably consider both wind and finite amplitude swell effects to explain the variability of α .

If this dissipation is due to the proposed air-sea friction mechanism, the associated momentum flux $\rho_w g E_s/2$ goes to the atmosphere. If underwater processes are involved, an energy flux $\rho_w g C_g E_s$ may go into ocean turbulence. Accordingly, these fluxes are small. For 3 m high swells, the momentum flux is only 8% of the wind stress produced by a 3 m s^{-1} wind. This momentum flux thus plays a minor role in observed O(50%) modifications of the wind stress at low wind [Grachev and Fairall, 2001]. Wind stress modifications are more likely related to a nonlinear influence of swell on turbulence in the atmospheric boundary layer [Sullivan *et al.*, 2008]. The dissipation coefficient α is a key parameter for models of this effect [Kudryavtsev and Makin, 2004; Hanley and Belcher, 2008].

5. Conclusions

Using high quality data from a space-borne synthetic aperture radar, ocean swells of periods 13 to 18 s were systematically tracked across ocean basins over the period 2003 to 2007. Among these, 12 storms provided enough data to allow a total of 28 estimations of the swell energy budget. The dissipation of small-amplitude swells is not distinguishable from viscous dissipation, with decay scales larger than 30000 km. On the contrary, steep swells lose a significant fraction of their energy, up to 65% over a distance as short as 2700 km. This non-linear behavior is consistent with a transition from a laminar to a turbulent air-side boundary layer. The present analysis opens the way for a better understanding of air-sea fluxes in low wind conditions. A satisfactory parameterization of this swell dissipation [Ardhuin *et al.*, 2008] was introduced in May 2008 in the global-scale wave forecasting research system operated by SHOM. Without wave data assimilation, this system still provides forecasts for swell-dominated regions, such as the U.S. West coast or North-West Australia, that are significantly more accurate in terms of wave heights than the operational systems developed earlier (see <http://www.jcomm-services.org/Wave-Forecast-Verification-Project.html>). Further investigations are necessary to understand the wind stress modulations and its variation with wind speed, direction, and swell amplitude. Such an effort is essential for the further improvement of numerical wave models.

Acknowledgments. All three authors contributed equally to the paper. SAR data was kindly provided by the European Space Agency (ESA), which also funded initial analysis work. The swell decay analysis was funded by the French Navy as part of the EPEL program. This work is a contribution to the ANR-funded project HEXECO and DGA-funded project ECORS. We thank the many contributors of in situ observations to the Joint Commission on Oceanography and Marine Meteorology (JCOMM) wave model intercomparison program, coordinated by J. Bidlot.

References

Ardhuin, F., and A. D. Jenkins (2006), On the interaction of surface waves and upper ocean turbulence, *J. Phys. Oceanogr.*, 36(3), 551–557.

Ardhuin, F., F. Collard, B. Chapron, P. Quefféulou, J.-F. Filippet, and M. Hamon (2008), Spectral wave dissipation based on observations: a global validation, in *Proceedings of Chinese-German Joint Symposium on Hydraulics and Ocean Engineering, Darmstadt, Germany*.

Babanin, A. V. (2006), On a wave-induced turbulence and a wave-mixed upper ocean layer, *Geophys. Res. Lett.*, 33(3), L20,605, doi:10.1029/2006GL027308.

Bidlot, J., S. Abdalla, and P. Janssen (2005), A revised formulation for ocean wave dissipation in CY25R1, *Tech. Rep. Memorandum R60.9/JB/0516*, Research Department, ECMWF, Reading, U. K.

Chalikov, D. (1993), Comments on "wave-induced stress and the drag of air flow over sea waves" and "quasi-linear theory of wind wave generation applied to wave forecasting", *J. Phys. Oceanogr.*, 23, 1597–1600.

Chapron, B., H. Johnsen, and R. Garello (2001), Wave and wind retrieval from SAR images of the ocean, *Ann. Telecommun.*, 56, 682–699.

Collard, F., F. Ardhuin, and B. Chapron (2005), Extraction of coastal ocean wave fields from SAR images, *IEEE J. Oceanic Eng.*, 30(3), 526–533.

Collard, F., B. Chapron, F. Ardhuin, H. Johnsen, and G. Engen (2006), Coastal ocean wave retrieval from ASAR complex images, in *Proceedings of OceanSAR*, Earth Observation Marine Surveillance Coordination Committee, Saint John's, Canada.

Darbyshire, J. (1958), The generation of waves by wind, *Phil. Trans. Roy. Soc. London A*, 215(1122), 299–428.

Dore, B. D. (1978), Some effects of the air-water interface on gravity waves, *Geophys. Astrophys. Fluid. Dyn.*, 10, 215–230.

Engen, G., and H. Johnsen (1995), Sar-ocean wave inversion using image cross spectra, *IEEE Trans. on Geosci. and Remote Sensing*, 33, 4.

Gerling, T. W. (1992), Partitioning sequences and arrays of directional ocean wave spectra into component wave systems, *J. Atmos. Ocean Technol.*, 9, 444–458.

Grachev, A. A., and C. W. Fairall (2001), Upward momentum transfer in the marine boundary layer, *J. Phys. Oceanogr.*, 31, 1698–1711.

Hanley, K. E., and S. E. Belcher (2008), Wave-driven wind jets in the marine atmospheric boundary layer, *J. Atmos. Sci.*, 65, 2646–2660.

Harris, D. L. (1966), The wave-driven wind, *J. Atmos. Sci.*, 23, 688–693.

Hasselmann, S., C. Brüning, and K. Hasselmann (1996), An improved algorithm for the retrieval of ocean wave spectra from synthetic aperture radar image spectra, *J. Geophys. Res.*, 101, 16,615–16,629.

Heimbach, P., and K. Hasselmann (2000), Development and application of satellite retrievals of ocean wave spectra, in *Satellites, oceanography and society*, edited by D. Halpern, pp. 5–33, Elsevier, Amsterdam.

Holt, B., A. K. Liu, D. W. Wang, A. Gnanadesikan, and H. S. Chen (1998), Tracking storm-generated waves in the northeast pacific ocean with ERS-1 synthetic aperture radar imagery and buoys, *J. Geophys. Res.*, 103(C4), 7917–7929.

Jensen, B. L., B. M. Sumer, and J. Fredsøe (1989), Turbulent oscillatory boundary layers at high Reynolds numbers, *J. Fluid Mech.*, 206, 265–297.

Johnsen, H., and F. Collard (2004), ASAR wave mode processing - validation of reprocessing upgrade. technical report for ESA-ESRIN under contract 17376/03/I-OL, *Tech. Rep. 168*, NORUT.

Johnsen, H., G. Engen, F. Collard, V. Kerbaol, and B. Chapron (2006), Envisat ASAR wave mode products - quality assessment and algorithm upgrade, in *Proceedings of SEASAR 2006*, SP-613, ESA, ESA - ESRIN, Frascati, Italy.

Kudryavtsev, V. N., and V. K. Makin (2002), Coupled dynamics of short waves and the airflow over long surface waves, *J. Geophys. Res.*, 107(C12), 3209, doi:10.1029/2001JC001251.

Kudryavtsev, V. N., and V. K. Makin (2004), Impact of swell on the marine atmospheric boundary layer, *J. Phys. Oceanogr.*, 34, 934–949.

Munk, W. H., and F. E. Snodgrass (1957), Measurements of southern swell at Guadalupe island, *Deep Sea Res.*, 4, 272–286.

Munk, W. H., G. R. Miller, F. E. Snodgrass, and N. F. Barber (1963), Directional recording of swell from distant storms, *Phil. Trans. Roy. Soc. London A*, 255, 505–584.

Raschle, N., F. Ardhuin, P. Quefféulou, and D. Croizé-Fillon (2008), A global wave parameter database for geophysical applications. part 1: wave-current-turbulence interaction parameters for the open ocean based on traditional parameterizations, *Ocean Modelling*, doi:10.1016/j.ocemod.2008.07.006.

Rogers, W. E. (2002), An investigation into sources of error in low frequency energy predictions, *Tech. Rep. Formal Report 7320-02-10035*, Oceanography division, Naval Research Laboratory, Stennis Space Center, MS.

Schulz-Stellenfleth, J., S. Lehner, and D. Hoja (2005), A parametric scheme for the retrieval of two-dimensional ocean wave spectra from synthetic aperture radar look cross spectra, *J. Geophys. Res.*, 110, C05,004, doi:10.1029/2004JC002822.

Snodgrass, F. E., G. W. Groves, K. Hasselmann, G. R. Miller, W. H. Munk, and W. H. Powers (1966), Propagation of ocean swell across the Pacific, *Phil. Trans. Roy. Soc. London*, A249, 431–497.

Sullivan, P. P., J. B. Edson, T. Hristov, and J. C. McWilliams (2008), Large-eddy simulations and observations of atmospheric marine boundary layers above nonequilibrium surface waves, *J. Atmos. Sci.*, 65(3), 1225–1244.

Tolman, H. L. (2002), Validation of WAVEWATCH-III version 1.15, *Tech. Rep. 213*, NOAA/NWS/NCEP/MMAB.

Tolman, H. L. (2003), Treatment of unresolved islands and ice in wind wave models, *Ocean Modelling*, 5, 219–231.

WISE Group (2007), Wave modelling the state of the art, *Progress in Oceanography*, 75, 603–674, doi:10.1016/j.pocean.2007.05.005.

Fabrice Ardhuin, Service Hydrographique et Océanographique de la Marine, 29609 Brest, France. (ardhuin@shom.fr)

Bertrand Chapron, Laboratoire d'Océanographie Spatiale, Ifremer, Centre de Brest, 29280 Plouzané, France. (bertrand.chapron@ifremer.fr)

Fabrice Collard, Collecte Localisation Satellites, division Radar, 29280 Plouzané, France. (Dr.fab@cls.fr)